infrastructures

MDPI

Article

Evaluating the Influence of Drying Shrinkage on Cracking Resistance of Massive Self-Compacting Concrete with Blast Furnace Slag Using Finite Element Method

Benson Kipkemboi [1,2,*] and Shingo Miyazawa [3,*]

[1] Graduate School of Engineering, Ashikaga University, Ashikaga 326-8558, Japan
[2] Kenya Industrial Research and Development Institute, Nairobi P.O. Box 30650-00100, Kenya
[3] Professor Emeritus, Ashikaga University, Ashikaga 326-8558, Japan
* Correspondence: kipkemboibenson@yahoo.com (B.K.); miyazawa.shingo@g.ashikaga.ac.jp (S.M.)

Abstract: The application of self-compacting concrete in massive structures is still low due to the perceived high cracking tendency associated with high shrinkage and heat of cement hydration. This conclusion is from short-term research work of up to 3 months after casting. The purpose of this study is to evaluate the influence of drying shrinkage on the cracking resistance of massive self-compacting concrete with blast furnace slag using a three-dimensional finite element method of analysis (3D FEM). The restraint stress experiment results of the self-compacting concrete beam under drying conditions are compared with those of similar concrete beam models obtained from 3D FEM analysis. The value of the reduction coefficient for Young's modulus of elasticity was proposed to consider the effect of stress relaxation due to creep in concrete. By using the proposed value of the reduction coefficient, thermal stress analysis was performed on a 1 m thick massive concrete wall member, and the cracking resistance of self-compacting concrete with different replacement ratios of blast furnace slag is discussed. By using the proposed reduction coefficient to evaluate concrete stress due to drying, the accuracy of thermal stress analysis results can be improved to a marginal error of ±15% from the experiment results. Also, the low-temperature rise caused by the high replacement ratio of blast furnace slag at 50% and 70%, respectively, contributed to improved cracking resistance. Furthermore, the optimum blast furnace slag replacement for better cracking resistance depends on the expected exposure condition of the structure.

Keywords: self-compacting concrete; drying shrinkage; restraint shrinkage stress; cracking resistance; 3D FEM analysis

check for updates

Academic Editor: Hong Wong

Received: 1 December 2024
Revised: 18 December 2024
Accepted: 30 December 2024
Published: 6 January 2025

Citation: Kipkemboi, B.; Miyazawa, S. Evaluating the Influence of Drying Shrinkage on Cracking Resistance of Massive Self-Compacting Concrete with Blast Furnace Slag Using Finite Element Method. *Infrastructures* **2025**, *10*, 11. https://doi.org/10.3390/infrastructures10010011

Copyright: © 2025 by the authors. Licensee MDPI, Basel, Switzerland. This article is an open access article distributed under the terms and conditions of the Creative Commons Attribution (CC BY) license (https://creativecommons.org/licenses/by/4.0/).

1. Introduction

When self-compacting concrete was first proposed by Dr. Hajime Okamura in Japan in 1986, it was regarded as a special type of concrete. Beginning in the early 1990s, several countries developed an interest in it, and its application gradually and rapidly became popular [1]. Since then, self-compacting concrete has evolved from the initial special type of concrete to a significantly essential type of concrete, driven by increasing technological advances that demand its use, e.g., in complex form structures, 3D concrete printing, and other innovative applications [2].

Despite the tremendous gains in popularizing self-compacting concrete, challenges still exist, among which include perceived low cracking resistance. The cracking resistance of concrete is the ability of the concrete to resist crack development and propagation.

Cracks in concrete constitute a pathway for the aggressive environmental media to attack concrete and influence its durability [3]. Studies have indicated that low cracking resistance in self-compacting concrete is associated with the high shrinkage and the high heat of cement hydration because of the high volume of paste used and low water-binder ratio as compared to normal concrete [4]. Due to this aspect, researchers are trying various solutions to mitigate this property, such as incorporating fibers such as micro steel fibers [5,6].

The design and production of self-compacting concrete requires a high volume of binders and superplasticizers to achieve flowability and self-compactability [7,8]. To reduce CO_2 emissions associated with ordinary Portland cement (OPC) production and to address other environmental concerns, many researchers have explored the use of various industrial by-product materials, such as fly ash and blast furnace slag, as a partial replacement for OPC in the production of self-compacting concrete [9–12].

The hydration heat of cement, which is associated with binder content and water-to-binder ratio, is the main factor that causes thermal stresses, which results in concrete cracking [13]. If stresses generated exceed concrete tensile strength, concrete cracks will occur [14]. Autogenous shrinkage strains caused by self-desiccation further increase stress and contribute to cracking in concrete. In conventional concrete, the autogenous shrinkage strain is generally not so large, but in concrete with a low water-cementitious materials ratio (w/c) or with silica fume it may be considerable [10]. With the decrease in the water-to-binder ratio (w/c) and the popularization of modern concrete, more attention has been given to autogenous shrinkage, self-desiccation, etc. [15]. These factors normally occur at an early age (within one week to two months after casting) of concrete.

In their past research, Tucry P et al. noted that there is no significant difference in total shrinkage between self-compacting concrete and ordinary concrete [16]. Thus, the effect of drying shrinkage on the cracking of concrete was not clearly established until recently when researchers like Ishikawa et al. demonstrated that drying shrinkage has a significant influence on concrete cracking [17]. Even so, the effect of extended drying shrinkage, especially on mass concrete structures, is still not so clear.

Thermal stress analysis in mass concrete structures has been a major problem since the 1960s [18]. With the advancement of technology, mechanisms, and establishments of prediction and control have strongly been pursued. Due to this, the FEM stress analysis program, called JCMAC3, used to calculate and predict restraint stress in concrete caused by temperature change due to heat of cement hydration and autogenous shrinkage, was developed by the Japan Concrete Institute (Japan Concrete Institute). This program has been widely used to control thermal cracking in massive concrete structures at an early age (within one week to two months after casting). In this program, a feature for analyzing the stress caused by the drying shrinkage of concrete was recently introduced after various research proposals indicated that drying shrinkage contributed significantly to concrete cracking [17]. It has not been quite clear what the contribution of drying shrinkage is to the cracking that normally occurs in massive self-compacting concrete with blast furnace slag subjected to drying for an extended period of time. It is expected that as drying continues, stress gradually decreases due to stress relaxation caused by the effect of creep [19].

To consider the stress relaxation effect due to creep, the program provides a conservative reduction factor to calculate the effective Young's modulus of elasticity. The application of this reduction factor works well for the thermal stress analysis of concrete within a short span of about 1 or 2 months. Thermal stress analysis for concrete members/specimens subjected to extended drying using the recommended factor gives unreasonably high stresses compared to the experimental stress results. In their attempt to find out the effects of this factor, Ryoichi A. et al. studied the thermal stresses of various concrete mixtures and

concluded that the factor is affected by the variation of hydration heat of cement [20]. Their study was, however, for a short curing period of less than a month.

This study, therefore, intends to evaluate precisely the influence of drying shrinkage on restraint stress of massive self-compacting concrete with blast furnace slag under extended drying using 3D FEM stress analysis. Experiments to determine adiabatic temperature rise, compressive strength, Young's modulus, and drying shrinkage were conducted, and the experimental results were used as input data for 3D FEM stress analyses. An experiment to find out restraint stress due to drying was carried out, and the results were compared with 3D FEM stress analysis results. A new procedure to consider the effect of stress relaxation due to the effect of creep in concrete was proposed for use in JCMAC3. Based on the stress analyses for a massive concrete model structure using the proposed reduction factor, the cracking resistance of self-compacting concrete with various replacements of blast-furnace slag is discussed. The general research outline is shown in Figure 1.

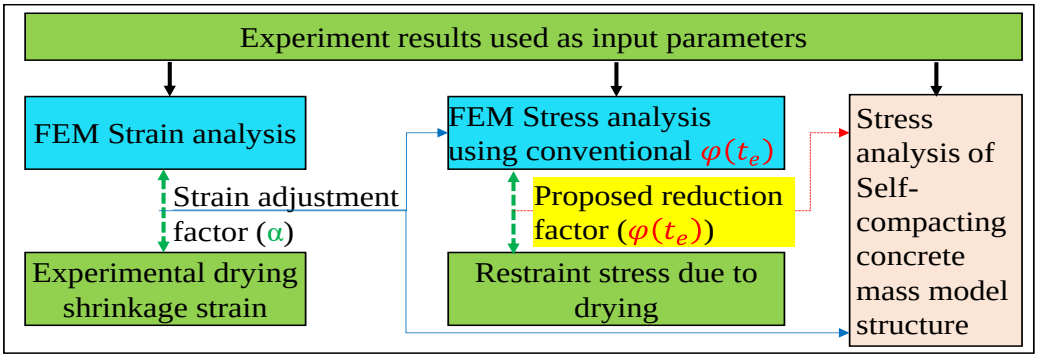


Figure 1. An overview of the research outline.

2. Materials and Methods

2.1. Materials Used

Ordinary Portland cement (N) conforming to JIS R 5210 was used in all mixtures. Ground granulated blast furnace slag (BFS) conforming to JIS A 6206 was used as a mineral admixture for partial replacement of OPC. In general, BFS with Blaine fineness in the range of 4000 cm^2/g is the most commonly used mineral admixture in Japan. The scanning electron microscope (SEM) images of OPC and BFS are shown in Figure 2. Fine and coarse aggregates conforming to ASTM C33 and JSCE 2012 standards were used [21,22]. River sand was used as fine aggregates with a specific gravity of 2.59 g/cm^3, percentage water absorption of 2.55%, and fineness modulus of 2.83. Coarse aggregates are from crushed sandstone with a maximum size of 20 mm and a specific gravity of 2.64 g/cm^3. A polycarboxylic-type high-range water-reducing and air-entraining agent (HRWAE) superplasticizer was used to enhance flowability, and the air entraining agent (AE) was used to keep the target air content. The chemical compositions and physical properties of the cementitious materials used are shown in Table 1.

Table 1. Physical and chemical properties of cementitious materials used.

Cementitious Materials	Density	Fineness	Chemical Composition (%)								
	(g/cm^3)	(cm^2/g)	ig-loss	SiO_2	Al_2O_3	Fe_2O_3	CaO	MgO	SO_3	Na_2O	K_2O
OPC (N)	3.16	3200	0.94	20.84	5.49	3.07	63.89	1.97	2.40	0.40	0.32
BFS	2.90	4590	0.16	32.30	13.93	0.42	42.97	5.68	2.06	0.17	0.29

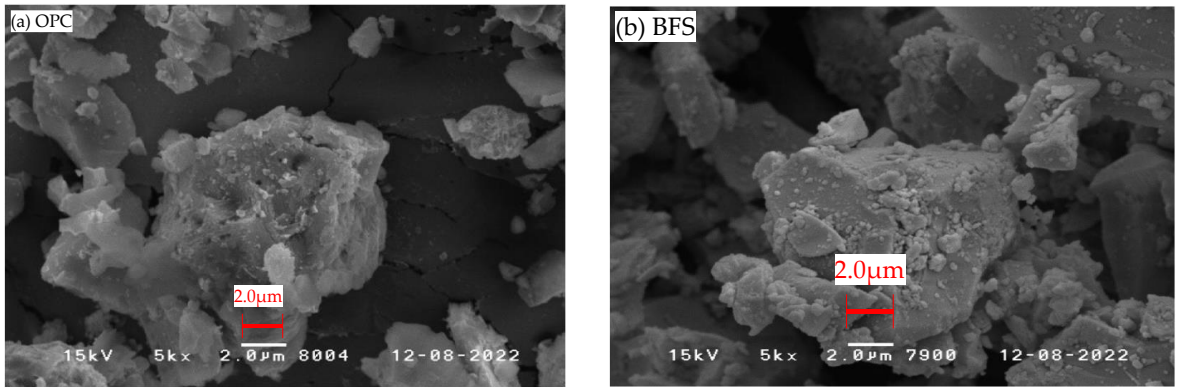


Figure 2. SEM images of OPC and blast furnace slag powder used in the experiment.

2.2. Mix Proportions of Concrete

The Japanese method of mix proportioning was adopted in the design of self-compacting concrete (SCC) as stipulated in JSCE 2012 guideline, and "rank 2" powder-type self-compacting concrete was prepared and used to cast the test specimen [23]. Rank 2 self-compacting concrete is concrete that can be self-compacted through minimum rebar clearance of 60 to 200 mm. This normally corresponds to a steel content of 350 to 100 kg/m^3. Target slump and air content were kept at 650 ± 50 mm and 4.5 ± 1.0%, respectively. Conventional concrete made from OPC was used as a control specimen. Material mix proportions are shown in Table 2, where W/B represents the water-to-binder ratio, and W/P represents the water-to-powder ratio as a volume percentage.

Table 2. Material mix proportions.

Mix Name	BFS Replacement Ratio (%)	W/B (%)	W/P in Volume (%)	Abs Agg. Vol (m^3/m^3)	Unit Contents (kg/m^3)					AE Cx%	HRWRAE Cx%
					Water W	Binder (B)		Aggregates			
						OPC	BFS	S	C.A		
SCC30	30	33.5	103	0.28	175	366	157	855	739	0.009	0.97
SCC50	50	32.0	97			273	273	828	739	0.012	0.73
SCC70	70	32.5	97			161	376	828	739	0.012	0.66
OPC(N)	0	55.0	174	0.36	180	327	-	812	957	0.001	1.0

2.3. Test Methods

2.3.1. Fresh and Hardened Properties of Concrete

Fresh properties of self-compacting concrete were tested to verify self-compactibility equivalent to rank 2 as per JSCE recommendation and concrete specimens prepared [23].

For the compressive strength test, specimens were cast on cylindrical molds 100 mm in diameter and 200 mm in depth. The specimens were cured under water at 20 °C, and strength test measurements were performed at the ages of 3, 7, 28, and 91 days according to ASTM C39/C39M-18 [24]. The casting temperature of all the samples was an average of 21 °C, with the max and min temperatures being 24.5 °C and 19 °C, respectively.

2.3.2. Heat of Cement Hydration

The temperature rise of concrete due to the heat of cement hydration was measured under semi-adiabatic conditions. Specimens were cast in insulation molds with internal dimensions of 400 mm in width, depth, and height, which were made of foamed polystyrene with a 200 mm thickness; the temperature of the central portion of concrete was measured as shown in Figure 3 using an embedded strain gauge. The room temperature was kept constant at 20 ± 1 °C throughout the experiment.

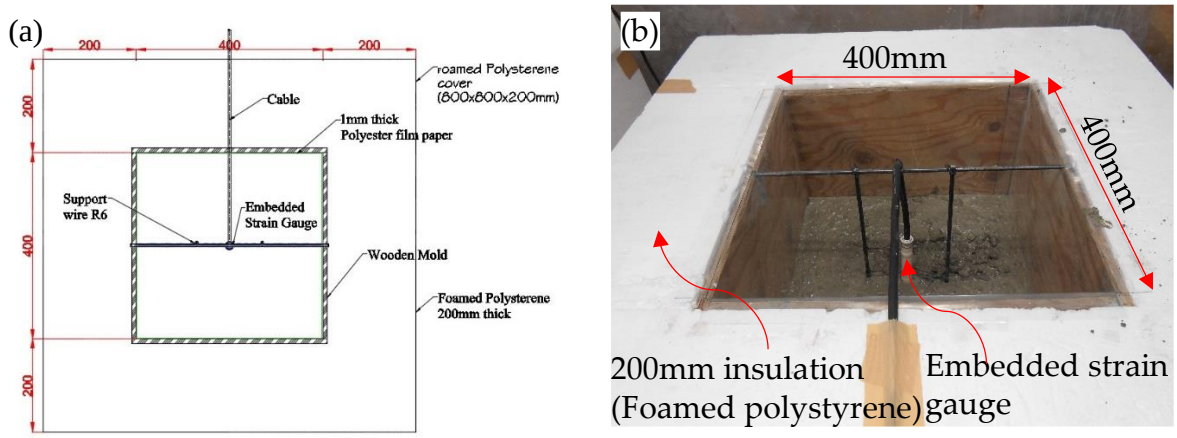


Figure 3. (**a**) Schematic plan view of the mold and (**b**) Specimen casting in the mold.

The adiabatic temperature rise of the concrete samples was determined using the observed semi-adiabatic temperature rise, and it was approximated by Equation (1) [25].

$$\rho CVT' - Sh\theta = \rho CV\theta' \quad (1)$$

where ρ is the density of the sample specimen (kg/m^3), C is the specific heat capacity of concrete taken as (1.05 KJ/kg °C), V is the volume of the sample specimen (m^3), and S is the surface area of the sample specimen (m^2). h is the heat transfer coefficient (W/m^2 °C) obtained as 0.403 for SCC30, 0.430 for SCC50, 0.485 for SCC70, and 0.450 for OPC. θ' is the rate of change of temperature per second and θ is the adiabatic temperature change with respect to constant room temperature. T is the temperature gradient existing between the sample specimen and the constant room temperature computed as a function of the above-described variables. In the specimens for semi-adiabatic temperature rise tests, the temperature difference between the center and surface of the concrete was very small, according to the preliminary experiments.

The adiabatic temperature rise of concrete can also be determined using the observed temperature rise under semi-adiabatic conditions and is approximated according to Equation (2) of the Guidelines for Control of Cracking of Mass Concrete, herein referred to as the JCI Guidelines 2017 [26]. Using a multi-component model for hydration heat, data are fitted using multiple regression analyses. The parameters Q_∞, r_{AT}, and S_{AT} are calculated as functions of cement type, unit content of cement, and placement temperature.

$$Q(t) = Q_\infty[1 - exp\left\{-r_{AT}\left(t - t_{0,Q}\right)^{SAT}\right\}] \quad (2)$$

where t = age (days), $Q(t)$ = adiabatic temperature rise (°C), Q_∞ = ultimate adiabatic temperature rise (°C), r_{AT} and S_{AT} = parameters representing rate of adiabatic temperature rise, and $t_{0,Q}$ = age at starting of temperature rise (days).

2.3.3. Autogenous Shrinkage

Autogenous shrinkage strains of self-compacting concrete specimens were carried out as proposed by the Japan Concrete Institute testing method, chapter 4 [27]. The autogenous strain was measured alongside semi-adiabatic temperature rise at the central portion of the specimen using an embedded strain gauge (which can measure strain and temperature rise simultaneously), as shown in Figure 3. Strain measurements were adopted after the initial setting time of each mixture. Autogenous shrinkage strain is calculated by subtracting thermal strain from observed strain. Thermal strain is calculated by multiplying temperature change with the coefficient of thermal expansion. The coefficient of thermal

expansion describes how the size of a material changes with a change in temperature and varies for each material. For concrete mixtures in this test, the coefficient of thermal expansion used was $10 \times 10^{-6}/°C$. The autogenous shrinkage strain of the OPC(N) concrete specimen was predicted using standard equations and constants from JCI Guidelines 2017 [26]. This is because OPC is one of the standard types of cement in Japan covered in the JCI guidelines, and autogenous shrinkage can be computed precisely without necessarily doing the experiment. This procedure is also described in our previous research [28].

2.3.4. Drying Shrinkage

For the drying shrinkage test, specimens were cast on molds of 100 × 100 × 400 mm, and the tests were carried out according to ASTM C157 [29]. The specimens were demolded after 1 day and cured under water at 20 ± 1 °C until 7 days after casting. Before the start of measurement, two contact cells were mounted centrally along the 400 mm length face at 300 mm apart, and the same was performed on the opposite face as gauge points. The length change of the specimen was measured between the attached contact cells on each face using a high-precision dial gauge. Two specimens were prepared for each mix proportion and stored at 20 ± 1 °C and R.H 60 ± 5%. Drying Shrinkage was measured at 0, 1, 7, 14, 28, 56, 91, and 180 days, as shown in Figure 4. Note that after 1 week, drying shrinkage and autogenous shrinkage are included in the measurement. Since the autogenous shrinkage of slender members (in this period) is much less than drying shrinkage, we refer to the shrinkage of concrete subjected to drying after 7 days as drying shrinkage [10].

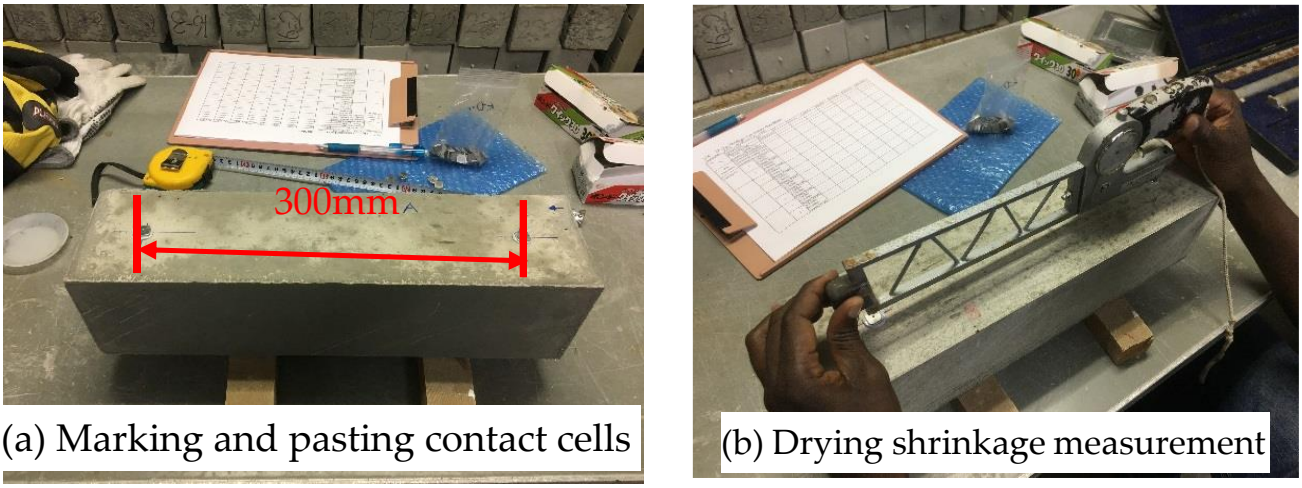


Figure 4. Setting and measurement of drying shrinkage strain.

2.3.5. Restraint Stress Due to Drying Shrinkage

For shrinkage cracking tendency, the restraint stress of concrete subjected to drying was measured by the uniaxial restraint stress test method as proposed by the Japan Concrete Institute, as shown in Figure 5 [27].

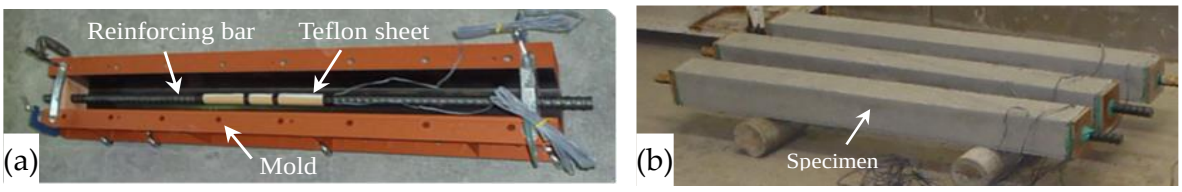


Figure 5. (**a**) Mold apparatus for shrinkage restraint stress test and (**b**) Specimen stored in drying condition.

A deformed rebar with a nominal diameter of 25 mm was embedded at the center of the concrete specimen of 100 × 100 × 1100 mm. Rebar ribs and lugs were removed within the central portion within 300 mm. Two strain gauges were attached unidirectionally, centrally, and on opposite diametric lines of the portion and sealed with 0.2 mm thick Teflon sheet to eliminate bonding between rebar and concrete. After casting concrete, samples were cured under sealed conditions for 7 days to simulate actual mass concrete structure other than under-water curing and then exposed to constant drying at 20 ± 1 °C and R.H 60 ± 5%. Measurements of strain on rebar were started and continued until the age of 180 days. The restraint stress of concrete was determined from the strain of the rebar measured by the attached strain gauges. A sudden decrease in the strain of the rebar indicates a crack on the concrete specimen.

3. Results and Discussions

3.1. Heat of Cement Hydration

The results in Figure 6 show the semi-adiabatic and adiabatic temperature rise of concrete specimens. The temperature increase in cast concrete is a result of the heat evolved through the heat of cement hydration. This characteristic property is responsible for thermal cracking in concrete structures at early ages [30]. The rate of adiabatic temperature rise is high in SCC30. This is because, in SCC30, the content of OPC in the binder is high. The hydration reaction in OPC is rapid at the initial stages due to a high C_3S content, thus a high rate of adiabatic temperature rise [28]. The maximum concrete temperature is high in SCC50, indicating that a lot of hydration heat is generated during the hydration reaction. This is due to the high amount of binder used. SCC70 concrete specimens have low maximum concrete temperature because of their high replacement ratio of blast furnace slag (BFS). Generally, conventional OPC concrete registered the lowest concrete temperature rise due to high w/c and low binder content used, while self-compacting concrete (SCC) registered a high-temperature rise due to low w/c and high amount of powder used [31]. The corresponding constants of the heat of cement hydration Q_∞ and r_{AT} of each mix proportion are shown in Table 3. These constants are necessary input parameters for thermal stress analysis to calculate thermal strain and stress.

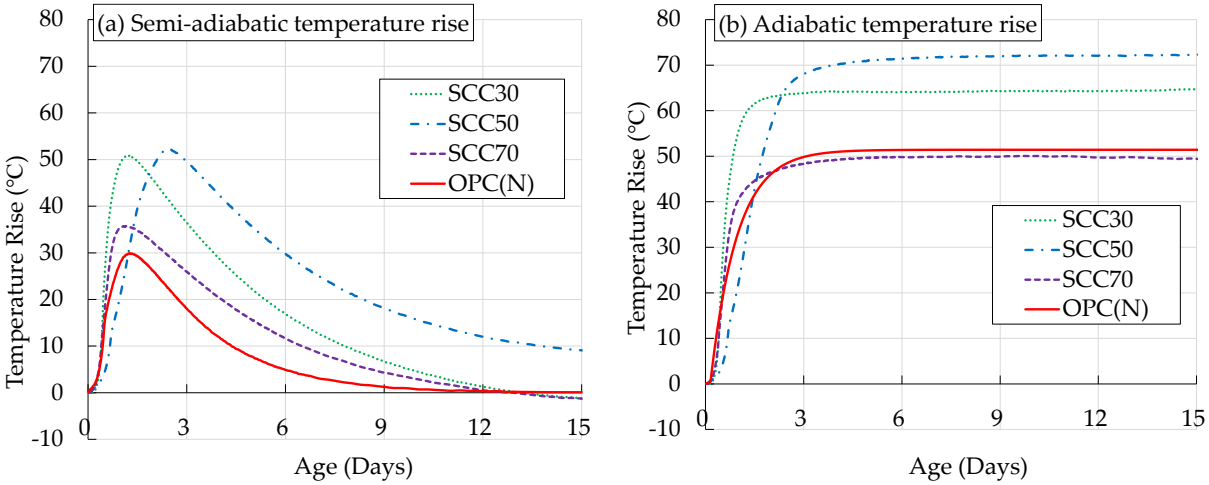


Figure 6. Semi-adiabatic and adiabatic temperature rise of concrete specimens.

Table 3. Input parameters of concrete properties for use in 3D FEM analysis.

Input Parameters	Mix Proportions			
	SCC30	**SCC50**	**SCC70**	**OPC(N)**
Thermal properties				
Coefficient of thermal conductivity (W/m°C)	2.7	2.7	2.7	2.7
Specific heat (KJ/kg°C)	1.15	1.15	1.15	1.15
Density of concrete (kg/m^3)	2295	2288	2280	2277
Ultimate adiabatic temperature rise Q_∞ (°C)	64.0	71.2	50.8	51.4
Temperature rise characteristic (r_{AT})	2.16	1.15	1.61	1.22
Effective age at start of heating (t,0) (days)	0.225	0.100	0.174	0.140
Mechanical properties				
28-day compressive strength (N/mm^2)	63.53	68.54	65.74	34.5
Coefficient (a)	3.204	7.12	3.542	3.686
Coefficient (b)	0.862	0.713	0.876	0.866
Setting time (S_f)—(days)	0.305	0.302	0.214	0.259
Tensile strength coefficient (C_1)	0.13	0.13	0.13	0.13
Tensile strength coefficient (C_2)	0.85	0.85	0.85	0.85
Modulus of elasticity coefficient (C_3)	6300	6300	6300	6300
Modulus of elasticity coefficient (C_4)	0.45	0.45	0.45	0.45
Poisson's ratio	0.2	0.2	0.2	0.2
Autogenous shrinkage	Raw experiment data			

3.2. Autogenous Shrinkage Strain

Autogenous shrinkage strain results are shown in Figure 7. Autogenous strain is the self-created bulk strain of cement paste, mortar, or concrete during and after hardening, excluding strain due to temperature change. In conventional concrete, autogenous shrinkage strain is not so large, but in concrete with a low water-to-cementitious materials ratio (w/c), it is considerably large [10]. The results in Figure 7 agree with this argument in that the autogenous shrinkage of SCC concrete samples with low w/c (0.3) has a high autogenous shrinkage strain as compared to that of OPC.

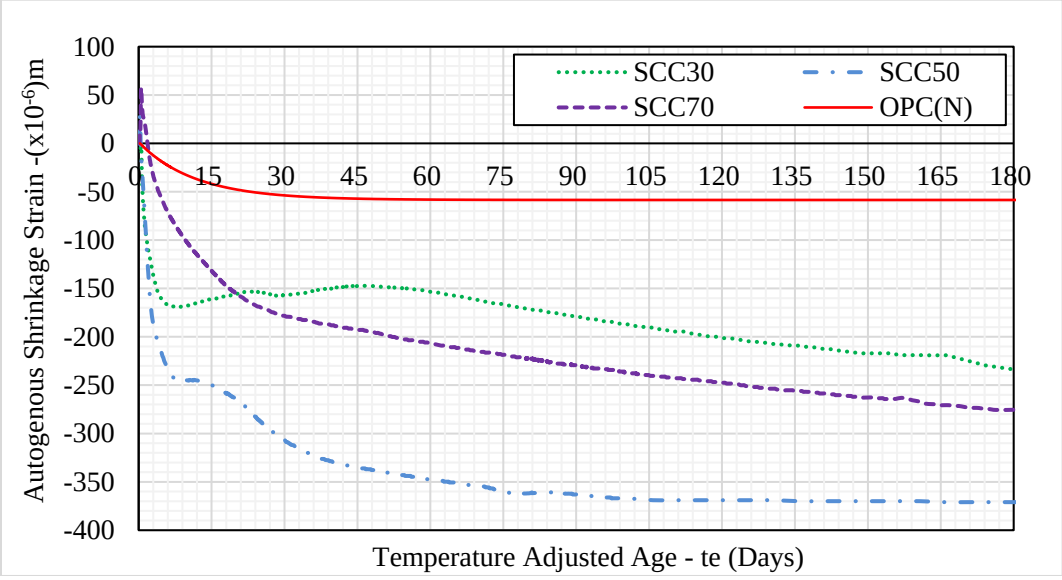


Figure 7. Autogenous shrinkage strain of concrete specimens.

In their research, Yang et al. suggested that concrete with a low water-to-cement ratio and large amount of binder, such as high-strength concrete and self-compacting concrete containing finely granulated blast furnace slag, exhibit significant autogenous shrinkage, which is due to hydration of the binder. This phenomenon is among the causes of crack generation in this type of concrete [32].

3.3. Drying Shrinkage Strain

Figure 8 shows the experimental drying shrinkage results of the concrete specimens over a period of six months. According to ACI concrete terminology, drying shrinkage in concrete is the decrease in length or volume change of the hardened concrete due to loss of capillary moisture [33]. This is a very important property in concrete materials since it also influences its durability.

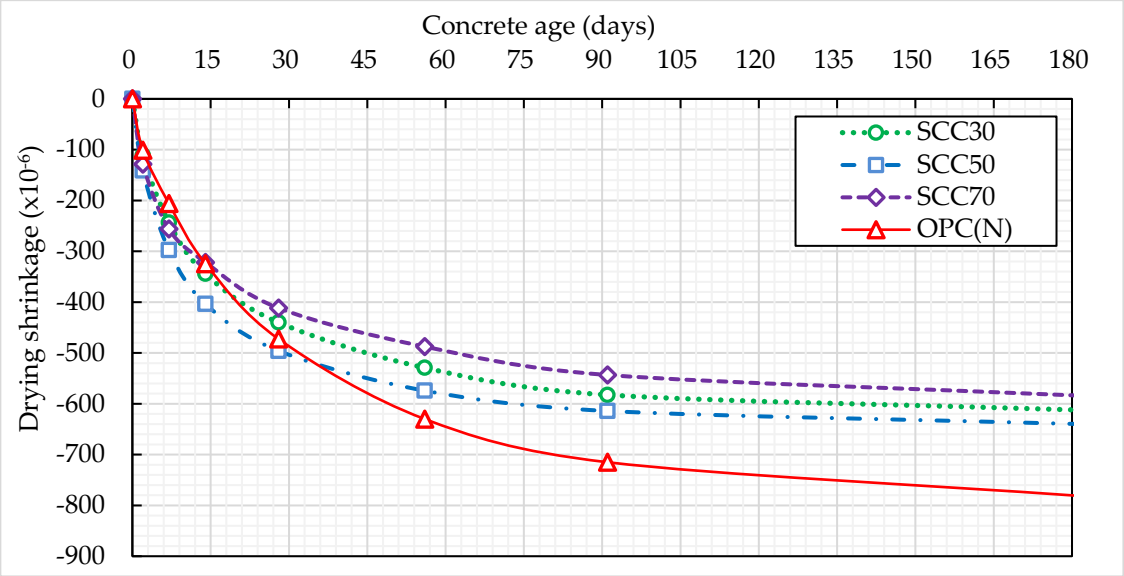


Figure 8. Experimental drying shrinkage strain of concrete specimens.

Recent research by Ishikawa et al. indicates that capillary moisture evaporation produces tensile stresses within concrete that lead to concrete cracking [17]. According to ASTM C157 and Japanese Architectural Standard Specification 5 (JASS5), 28 days of acceptable drying shrinkage needs to be under 500 and 800 micro-strains, respectively, for cracking safety [29]. This is on the assumption that after 28 days, concrete has attained enough strength and that the influence of drying shrinkage is insignificant. In this experiment, concrete specimens tested meet this 28-day specification requirement, with SCC50 experiencing the highest drying shrinkage strain (473 μm). Thereafter, after 28 days, as drying continues, drying shrinkage strain keeps increasing. The drying shrinkage trend is maintained by self-compacting concrete, while the drying shrinkage rate for OPC becomes higher until the age of 180 days, when its drying shrinkage strain is 782 μm. Results also indicate that a low water-to-binder ratio in SCC is significant in mitigating drying shrinkage because there is hardly any free pore water available for evaporation [17]. Considering the effects of the mineral admixture (BFS) replacement ratio, it can be seen that a high replacement ratio, i.e., 70% of BFS (SCC70), has low drying shrinkage strain. This result agrees well with the findings of Jamila M.A et al., in which a 60% replacement of fly ash reduced the drying shrinkage of self-compacting concrete [34].

3.4. Restraint Stress Due to Drying Shrinkage

In this study, the restraint stress of SCC30, SCC50, SCC70, and OPC(N) concrete samples subjected to drying at 20 °C and 60% R.H. was measured. The test results of the restraint stress of concrete are shown in Figure 9, in which the results of each mixture are expressed as positive values on the vertical (Y) axis. Since the specimens were subjected to drying from the age of 7 days, the restraint stress observed before 7 days is ignored since it is predominantly caused by autogenous shrinkage. This is because free autogenous

deformation expands within 1 day and shrinks rapidly from 3 days to 7 days, and the resultant strains almost cancel out [19]. From the age of 7 days, both autogenous shrinkage and drying shrinkage occur steadily and are the cause of restraint stress, with drying shrinkage being the dominant factor for these mixtures.

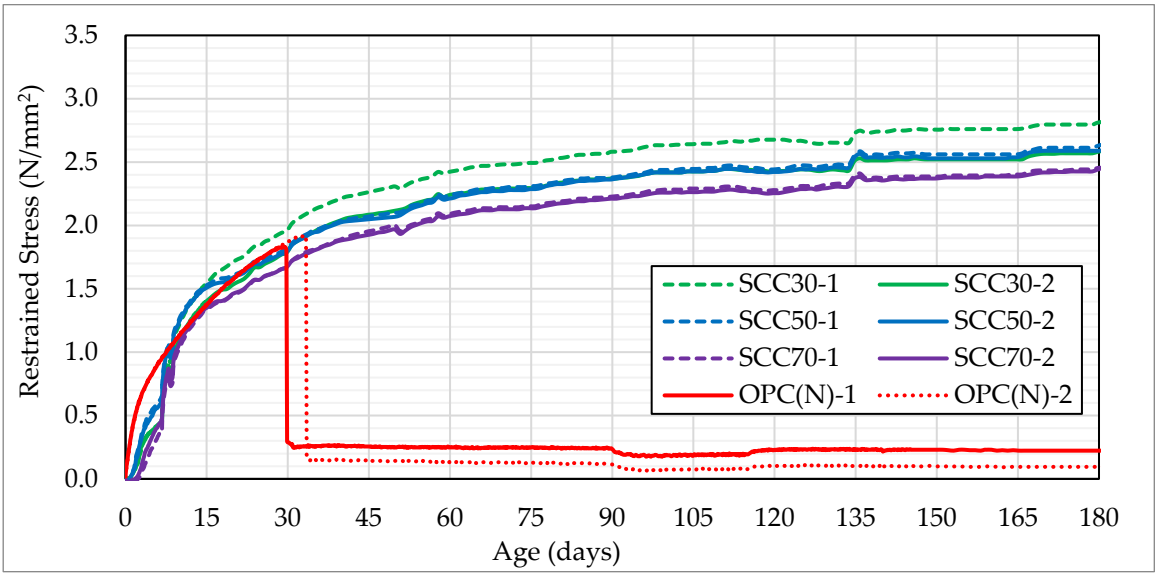


Figure 9. Restraint stress of concrete specimens subjected to drying shrinkage.

It can be seen from the figure that restraint stresses increased steadily with drying. After about one and a half months of drying, the rate at which stress increases is reduced due to the effect of creep [19].

Considering the effect of BFS replacement ratios on restraint stress due to drying, stress build-up in SCC30 is higher (2.7 N/mm^2) than in SCC50 and SCC70. This is because of a high amount of OPC, which generates a lot of heat from cement hydration that causes more stress. A high replacement ratio of BFS (SCC50 and SCC70) reduces drying shrinkage stress due to the increased presence of calcium silicate (hydration product from BFS) in the mixture, which effectively contributes to a reduced porosity and densifies the matrix, thus mitigating extensive drying [35]. Compared with normal OPC concrete (N), cast without any BFS replacement, it took the shortest time (30 days) before cracks were seen. This indicates that SCC with BFS and a low w/b ratio is able to reduce restraint drying shrinkage stress and improve cracking resistance better than normal OPC concrete. The resistance to shrinkage cracking caused by thermal, autogenous, and drying shrinkage of self-compacting concrete with BFS cement is discussed in the succeeding section.

3.5. Restraint Stress Analysis by 3D Finite Element Analysis Method

3.5.1. General Outline of Stress Analysis by 3D Finite Element Analysis Method

Stress analysis by 3D FEM analysis was carried out using a computer program (JC-MAC3), as outlined in Figure 10. Input parameters as obtained from experiments are highlighted in green. In the analysis, stress relaxation due to creep for concrete subjected to drying shrinkage was considered using a conventional reduction factor $\varphi(t_e)$ for effective Young's modulus. The analysis results are compared with experimental results (restrained stress and drying shrinkage). The influence of creep on concrete stresses is evaluated using effective Young's modulus, which is obtained by multiplying Young's modulus by a reduction coefficient $\varphi(t_e)$. Typically, the reduction coefficient used is 0.42 from casting until the age when the concrete temperature reaches the maximum and 0.65 at later ages, as recommended by JCI guidelines 2008 [18]. In this study, a new procedure to consider stress

relaxation due to the effect of creep in concrete is proposed by modifying the conventional reduction coefficients. The newly proposed reduction factor, $\varphi(t_e)$, was used to precisely evaluate the influence of drying shrinkage on the stress of massive concrete structures subjected to up to 6 months of drying.

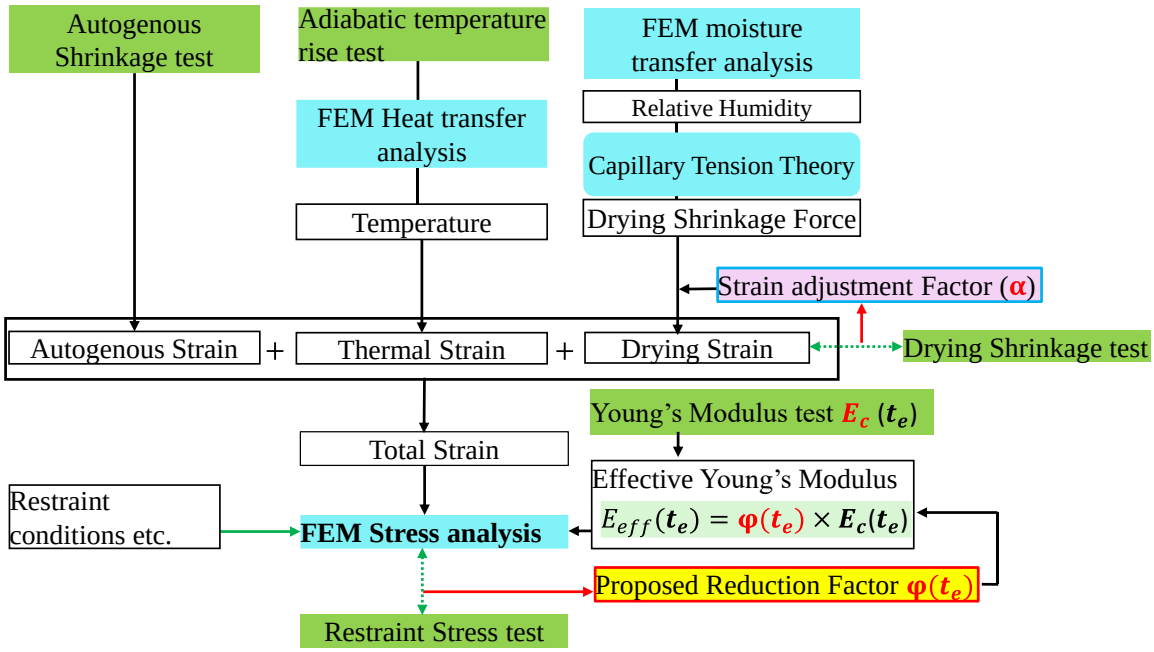


Figure 10. Outline of the flow steps in 3D FEM analysis of strain and stress in concrete.

3.5.2. Restraint Stress Due to Temperature Change and Autogenous Shrinkage

Stress analysis by the 3D FEM program (JCMAC3) was performed based on experimental results of concrete properties as input parameters. In thermal stress analysis, the transient heat transfer analysis was carried out using the experimental adiabatic temperature rise of each mixture. Each of the mix proportions has a different set of input parameters, as summarized in Table 3. A constant initial temperature of 20 °C was used for all the mixtures.

In thermal stress analysis, autogenous shrinkage strain is added to thermal strain, and linear elastic analysis is carried out by using Young's modulus (E_c) proposed by the Japan Concrete Institute; stress relaxation due to creep of concrete was considered by using effective Young's modulus (Ee_{ff}), as described in Equation (6) [18]. The tensile strength and Young's modulus of concrete in each mixture were determined from the observed compressive strength using Equation (3) and Equation (4), respectively, as per JCI Guidelines 2017 [26]. Tensile strength is used to calculate the cracking index, which is an indicator of cracking tendency.

$$f_t(t_e) = C_1 \times f'c(t_e)^{C2} \quad (3)$$

$$E_C(t_e) = C_3 \times f_c'(t_e)^{C4} \quad (4)$$

where f_t (t_e) is the tensile strength of concrete at t_e (N/mm^2), f_c' (t_e) is the compressive strength of the concrete at t_e (N/mm^2), E_c (t_e) is the modulus of elasticity at t_e (N/mm^2), C_1, C_2, C_3, and C_4 are the constants recommended by JCI guidelines 2016 to be 0.13, 0.85,

6300 and 0.45, respectively, and t_e is the temperature adjusted age in days and is computed according to Equation (5).

$$t_e = \sum_{i=1}^{n} \Delta t_i \times exp\left[13.65 - \frac{4000}{273 + T(\Delta ti)/T_0}\right] \quad (5)$$

where Δt_i is the period of constant temperature continuing in concrete (day), T (Δt_i) is the concrete temperature for Δt_i (°C), and T_0 is 1 °C.

Stress relaxation and creep are time-dependent variables in concrete. External load or stress applied to the specimen may relax gradually due to the time-dependent properties of concrete [36]. To consider stress relaxation due to creep, a reduction factor—$\varphi(t_e)$ is introduced and multiplied by Young's modulus of concrete, as shown in Equation (6). This reduction coefficient is taken to be 0.42 until the maximum temperature is reached at the adjusted temperature age t_e and 0.65 at later ages, from one day after the maximum temperature, $\varphi(t_e)$ is linearly interpolated between 0.42 and 0.65 for the one-day gap. It is noted that $\varphi(t_e)$ is taken to be the smaller value during the temperature increase stage than after the time at the maximum temperature since stress relaxation of concrete is more significant at very early ages than at later age. Large stress relaxation of early-age concrete was also experimentally investigated by other researchers [19,20].

$$E_{eff}(t_e) = \varphi(t_e) \times E_c(t_e) \quad (6)$$

where $E_{eff}(t_e)$ is the effective modulus of elasticity of concrete at t_e, $E_c(t_e)$ is the modulus of elasticity of concrete at t_e, and $\varphi(t_e)$ is the reduction factor for the modulus of elasticity of concrete.

3.5.3. Consideration of Drying Shrinkage of Different Mixtures

Drying shrinkage of concrete is affected mostly by the properties of the materials used and environmental conditions. It has been shown that the type of coarse aggregates used is also one of the dominating factors affecting concrete drying shrinkage [37]. In order to consider the effect of the variations in each mix proportion on the drying shrinkage of concrete, adjustment factor (α) is introduced and used in JCMAC3. During FEM analysis, the free drying shrinkage strain of each element is multiplied by the adjustment factor (α) [38]. M. Ishikawa and K. Nijis proposed to use pore size distribution of hardened cement paste to predict free drying shrinkage of typical mixtures in JCMAC3 [17]. However, pore size distribution is not a generally obtained information. Therefore, in this study, the standard drying shrinkage test procedure using a 100 × 100 × 400 mm specimen is used to consider the effect of the mixture on drying shrinkage instead of pore size distribution.

In order to obtain adjustment factor (α), FEM analyses were performed, in which an eighth portion of the beam model (50 × 50 × 200 mm) corresponding to experimental drying shrinkage beam specimen (100 × 100 × 400 mm) was used as shown in Figure 11. To calculate the drying shrinkage strain in members and structures, the program performs FEM moisture transfer analysis was used to obtain the relative humidity of each element. Then, the radius of evaporated capillary pore water is computed based on pore size distribution and drying shrinkage force in the remaining capillary pore water. Based on capillary tension theory, the free drying shrinkage strain of each element is computed. Using pore parameters of each mix proportion and capillary tension theory, drying shrinkage force is computed. This concept is based on the general fact that when the water existing inside the pore evaporates, tensile force is exerted, which acts by pulling the walls of the pores towards each other. In this analysis, typical pore size distribution for normal concrete with a water-to-cement ratio of 45%, reported by M. Ishikawa, was used [17].

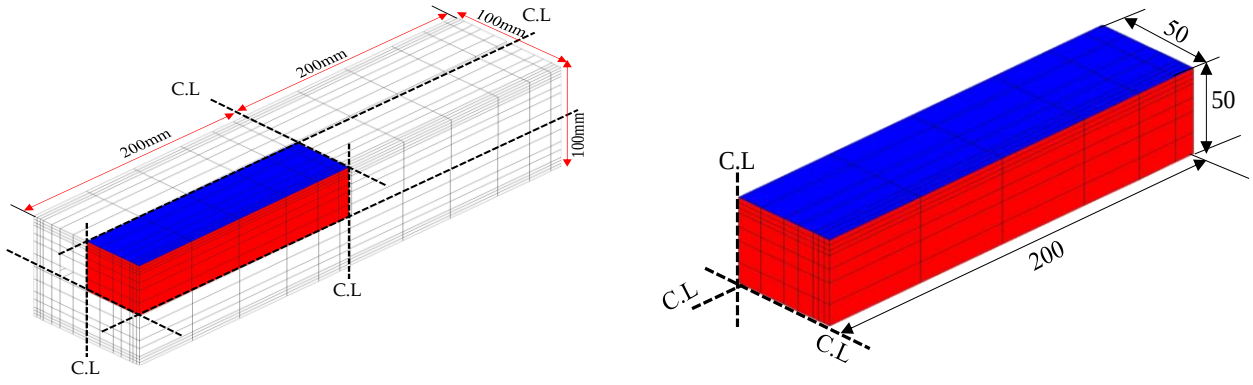


Figure 11. 3D FEM beam model structure for drying shrinkage strain.

The drying shrinkage strain of the specimen from FEM analysis is then compared with experimental drying shrinkage, and the appropriate strain adjustment factor (α) is computed. This factor is unique to each mix proportion. Thermal strain and autogenous strains are also computed using heat of cement hydration and autogenous shrinkage data of each mix proportion, respectively. These strains are much less than drying shrinkage strains in the specimens with such a small dimension and under drying conditions [39].

Results of 3D FEM analysis for the drying shrinkage strain of the specimens are shown in Figures 12–15. In this study, the strain adjustment factor (α) was determined so that the drying shrinkage of the specimen from FEM analysis fits the experimental value after 180 days of drying. However, the rate of drying shrinkage from the FEM results is larger than that from the experiment. The difference is attributed to the fact that a similar pore size distribution was used for each mixture in FEM analysis. In the future, for more precise calculation, it is recommended to measure and use the pore size distribution of each mixture.

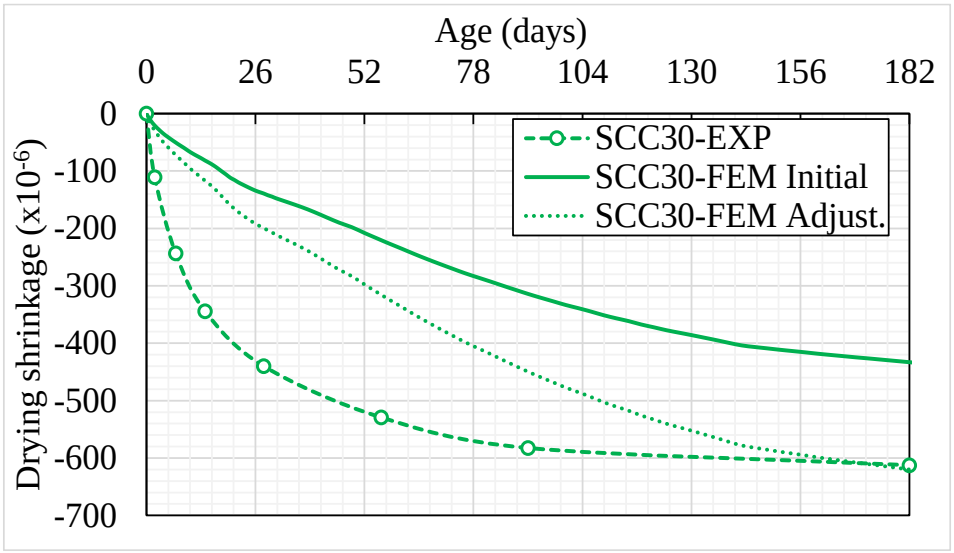


Figure 12. Adjustment of SCC30 FEM strains.

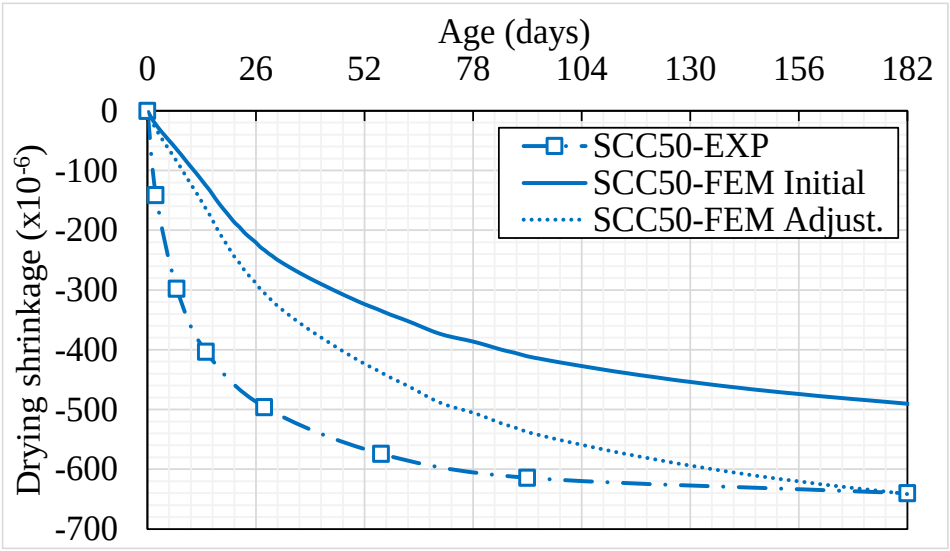


Figure 13. Adjustment of SCC50 FEM strains.

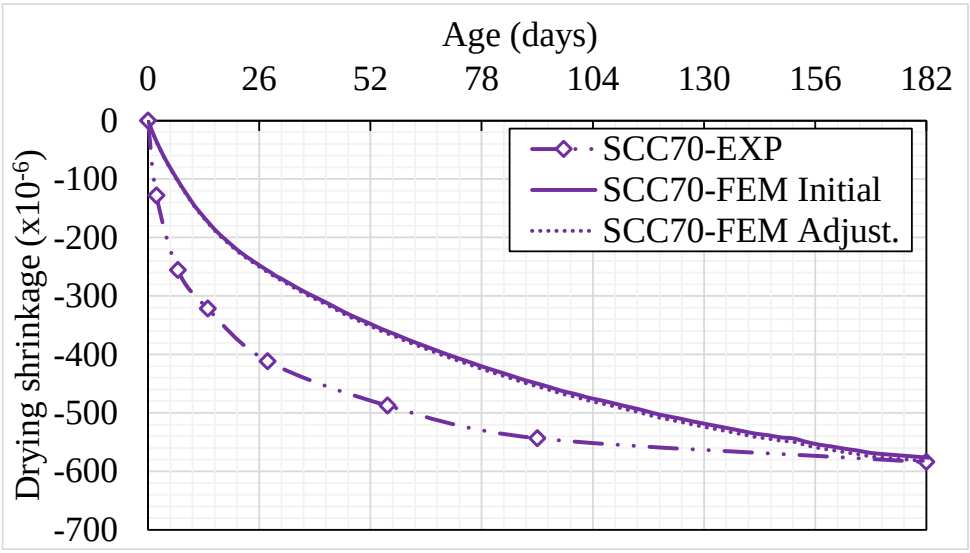


Figure 14. Adjustment of SCC70 FEM strains.

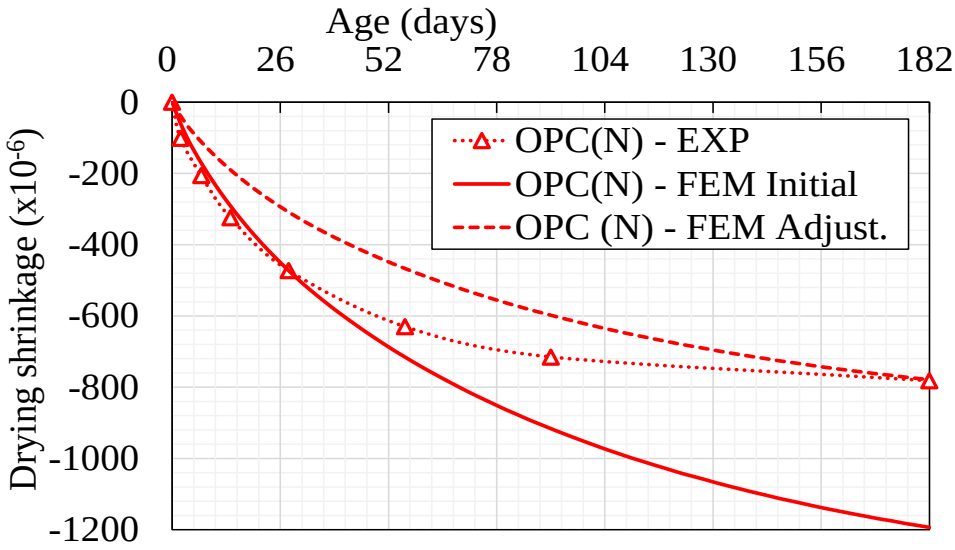


Figure 15. Adjustment of OPC(N) FEM strains.

The adjustment factors for each mix proportion are shown in Table 4. These factors are utilized in the restrain stress analysis described. The trend in FEM analysis strain is similar to the trend in experimental strains. Self-compacting concrete exhibits low drying shrinkage strain compared with OPC concrete.

Table 4. Strain adjustment factors (α) in FEM analysis for drying shrinkage.

Mix proportion	SCC30	SCC50	SCC70	OPC(N)
Adjustment factor	1.43	1.31	1.01	0.65

3.5.4. Restraint Stress Due to Drying Shrinkage

For 3D FEM analysis of restraint stresses in the beam specimen (100 × 100 × 1100 mm) due to drying shrinkage, An eighth portion of the beam model was used, as shown in Figure 16. Corresponding experimental data of each mix proportion, such as autogenous shrinkage, adiabatic temperature rise, drying shrinkage, and material properties necessary for analysis, are input. In addition, the adjustment factor obtained from strain adjustment is included as input data. Restraint stresses due to drying for each mix proportion are analyzed. 3D FEM analysis stresses and experimental restraint stresses due to the drying of each mix proportion were compared, and an appropriate reduction factor, $\varphi(t_e)$, for an effective Young's modulus of elasticity was proposed. This is a factor that can obtain an output stress almost the same as the experiment stress. This factor is independent of the individual mix proportions.

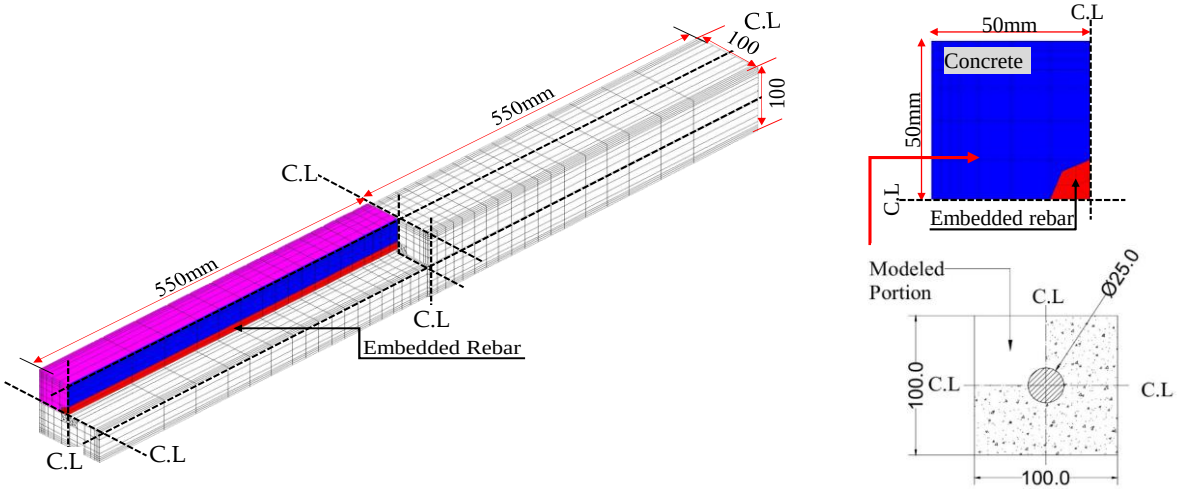


Figure 16. 3D FEM beam model structure for restraint stresses due to drying shrinkage.

Note that to calculate restraint stresses due to temperature change and autogenous shrinkage, a conventional reduction factor, $\varphi(t_e)$, proposed by JCI guidelines, is used to compute effective Young's modulus of elasticity, $E_{eff}(t_e)$ [18]. The dotted line shown in Figure 17 is the conventional reduction factor $\varphi(t_e)$. This conventional value $\varphi(t_e)$ is normally sufficient for stress analysis in concrete within a short period of a few weeks after casting to about 2 months [26]. Ryoichi A. et al. proposed a reduction factor of Young's modulus of early-age concrete younger than 2 weeks, but they did not study the value of $\varphi(t_e)$ for concrete subjected to drying for an extended period of time [20]. When the conventional reduction factor $\varphi(t_e)$ is used, the calculated restraint stresses increase more rapidly, contrary to the experimental results.

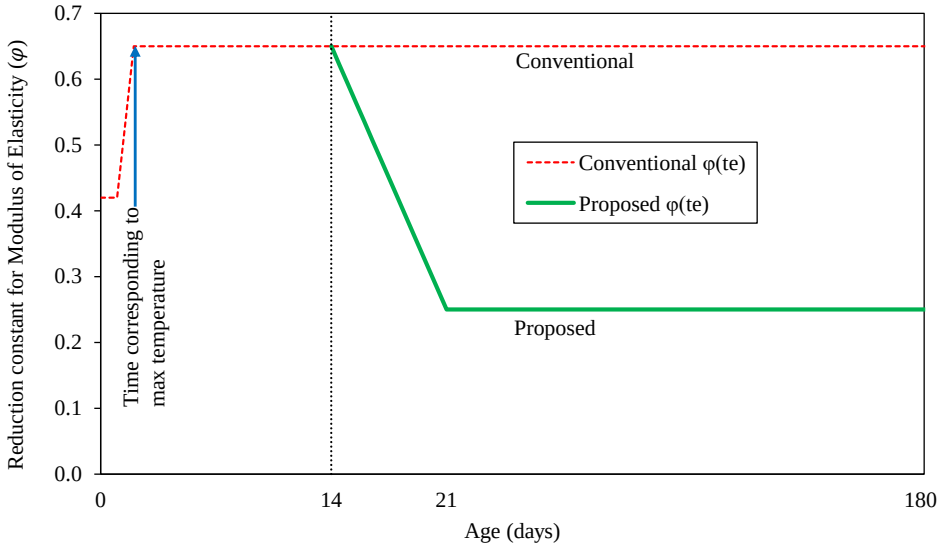


Figure 17. Proposed reduction coefficient for modulus of elasticity of concrete.

The proposed value of $\varphi(t_e)$ was assumed to be constant for each mixture, as is the case for the conventional value of $\varphi(t_e)$; it was determined that the analyzed stress approximately agrees with those obtained by the experiments.

The analysis and experimental results are compared and shown in Figures 18–21. It can be seen that the calculated stress using the proposed value of $\varphi(t_e)$ has better results than using the conventional value of $\varphi(t_e)$. The proposed value is able to accurately compute stresses to a marginal error of ±15% from the experimental results. It is noted that the value of $\varphi(t_e)$ is taken to be a relatively small value, as shown in Figure 17. Since drying shrinkage increases very slowly for an extended period, effective Young's modulus should be a considerably small value in elastic analysis to consider the large effect of creep of concrete. From the results, It can be said that the new proposed reduction coefficient precisely evaluates the restraint stress of self-compacting concrete subjected to long-term drying.

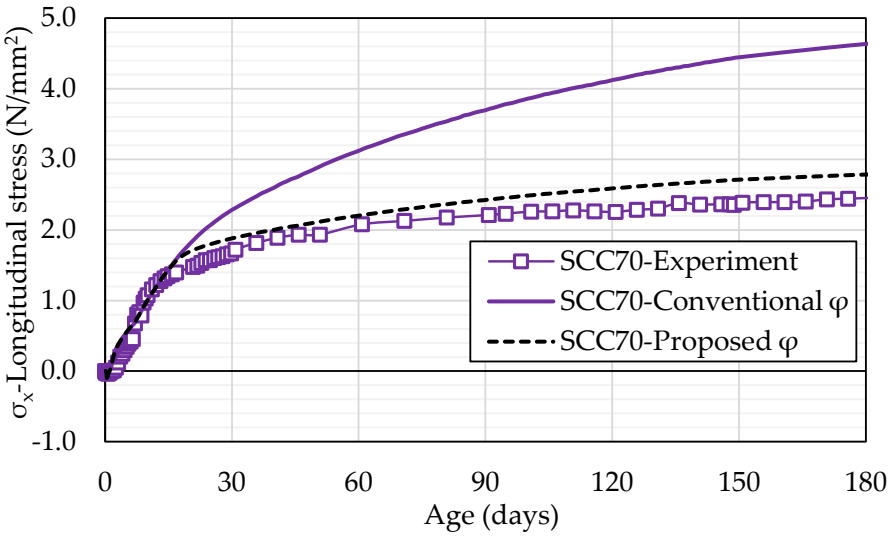


Figure 18. Proposed FEM analysis stress for SCC70.

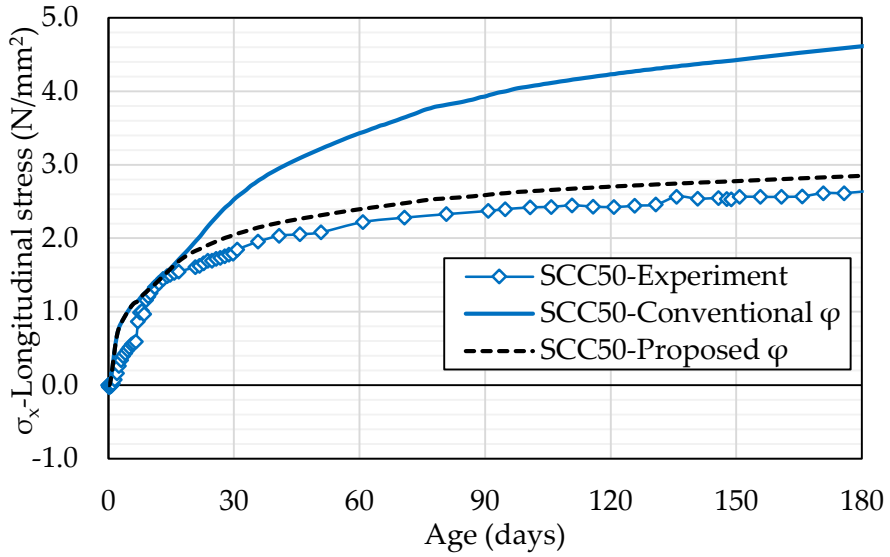


Figure 19. Proposed FEM analysis stress for SCC50.

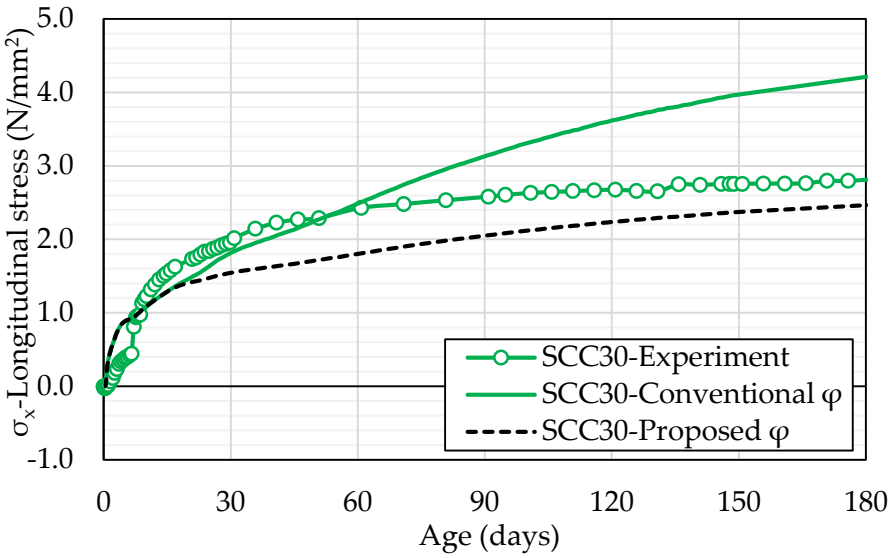


Figure 20. Proposed FEM analysis stress for SCC30.

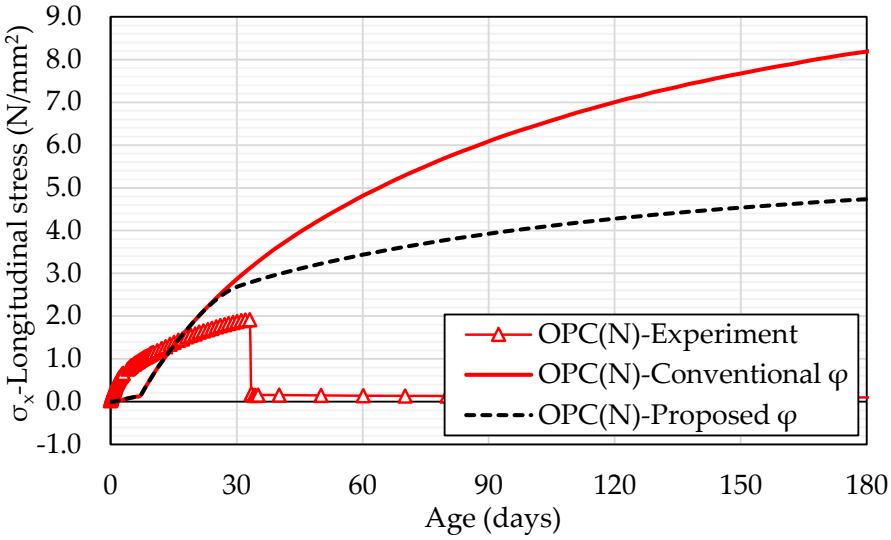


Figure 21. Proposed FEM analysis stress for OPC(N).

3.6. Estimation of Cracking Resistance of Self-Compacting Concrete Mass Structure Considering Drying Shrinkage

3.6.1. Mass Concrete Model Structure for Restraint Stress Analysis

In order to discuss the cracking resistance of massive self-compacting concrete in actual concrete structure applications, FEM analyses were carried out to simulate the restraint stress due to temperature change, autogenous shrinkage, and drying shrinkage generated in the wall-type model structure, as shown in Figure 22.

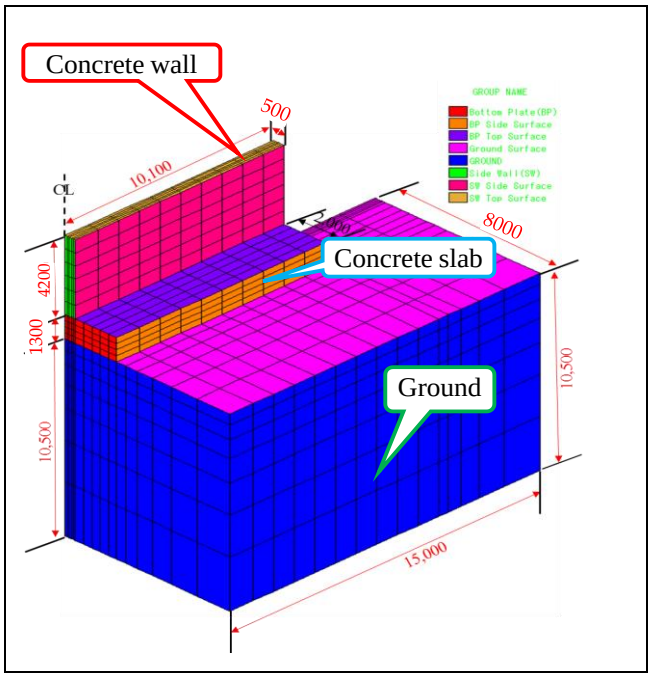


Figure 22. Model structure of actual wall mass concrete for use in 3D FEM (A quarter portion).

The thickness of the wall is 1.0 m, the height is 4.2 m, and the length is 20.2 m. In FEM analysis, one-fourth model is used. Wall concrete is cast one month after slab concrete was cast, and the wall is subject to drying in the atmospheric conditions at 20 °C and 60% relative humidity after formwork removal at the age of 7 days. In the future, the actual drying condition of a given place or region should be considered for analysis. The coefficient of heat transfer of the mold is assumed to be 14 W/m^2 °C. The experimental concrete properties of each mixture shown in Table 3 were used. The proposed reduction factor, $\varphi(t_e)$, was used to evaluate the influence of drying shrinkage for a period of up to 180 days. Analysis results indicate that tensile restraint stress in the longitudinal direction generated in the wall member is dominant. These stresses are discussed as the main cause of cracking in this type of structure.

In order to evaluate the cracking tendency of mass concrete structures, the cracking index is used. The cracking index is defined as the ratio of the tensile strength of concrete to tensile stresses as shown in Equation (7), which is proposed by JCI 2016 Guidelines for the control of cracking of mass concrete.

$$I_{cr} = \frac{f_t(t_e)}{\sigma(te)_{max}} \tag{7}$$

where I_{cr} is the cracking index, $ft(t_e)$ is the tensile strength (N/mm^2), $\sigma(t_e)_{max}$ is the maximum principal stress (N/mm^2), and t_e is the temperature-adjusted age (day).

3.6.2. Cracking Resistance of SCC Mass Concrete at Early Age

For crack control in mass concrete structures, restraint stress caused by temperature change due to cement hydration and autogenous shrinkage is generally analyzed for the period from 1 to 2 months. This period is dependent on the thickness of the member, and about 1 month is recommended by JCI Guidelines for the size similar to the current model structure [18]. Results from 3D FEM analysis show that at about 1 month, the critical region with low cracking resistance is at the center (core) of the structure, as shown in Figure 23, and agrees well with the trend in our previous research [10]. This trend is largely influenced by the heat of cement hydration and autogenous shrinkage, which produces dominant cracking stresses. The temperature rise due to cement hydration is higher in the core than the surface of the wall. This results in larger thermal shrinkage, which corresponds to a large temperature decrease. This non-uniform strain in the cross-section leads to an increase in tensile stresses at the core, which is caused by internal restraint.

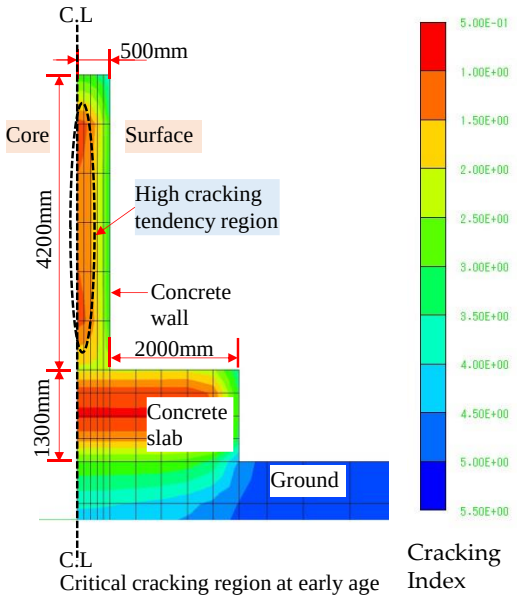


Figure 23. High cracking tendency region of the concrete wall structure at an early age.

At the core of the structure, the stresses are higher, as shown in Figure 24. Generally, self-compacting concrete develops high stresses as compared with OPC. The trend of stresses generated corresponds to that of heat of cement hydration. This is due to the high heat of cement hydration caused by the high amount of binder content and a low water-to-binder (w/c) ratio.

The cracking index analysis of the wall structure at the core indicates that the three mixed proportions of self-compacting concrete have a lower cracking index than the control specimen (OPC), as shown in Figure 25. This shows that self-compacting concrete has a low cracking resistance at an early age compared to OPC. SCC70 has the highest cracking resistance. This is because of the high replacement ratio of blast furnace slag. SCC50 has the lowest cracking index, indicating a low cracking resistance. This is because of the high restraint stresses occasioned by high autogenous shrinkage. After a short period of about 10 days, the cracking index in all mixtures drops significantly before becoming constant. The significant drop is associated with the temperature changes that occur when concrete temperatures decrease. The core is not affected by the drying condition, which occurs at the surface of the member since a thick layer of concrete acts as an insulation.

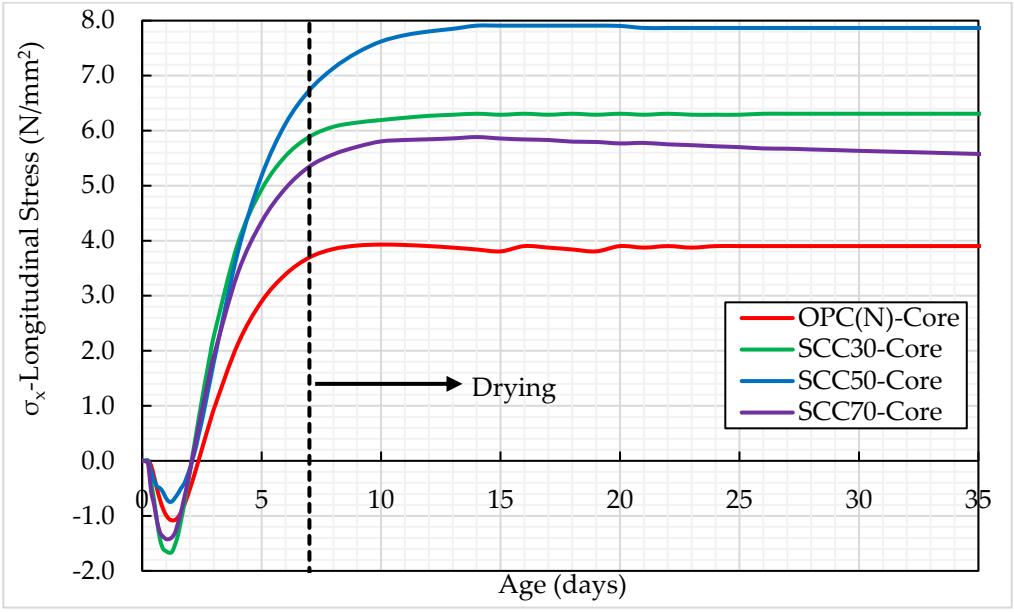


Figure 24. Stresses at the core of the concrete wall structure at an early age.

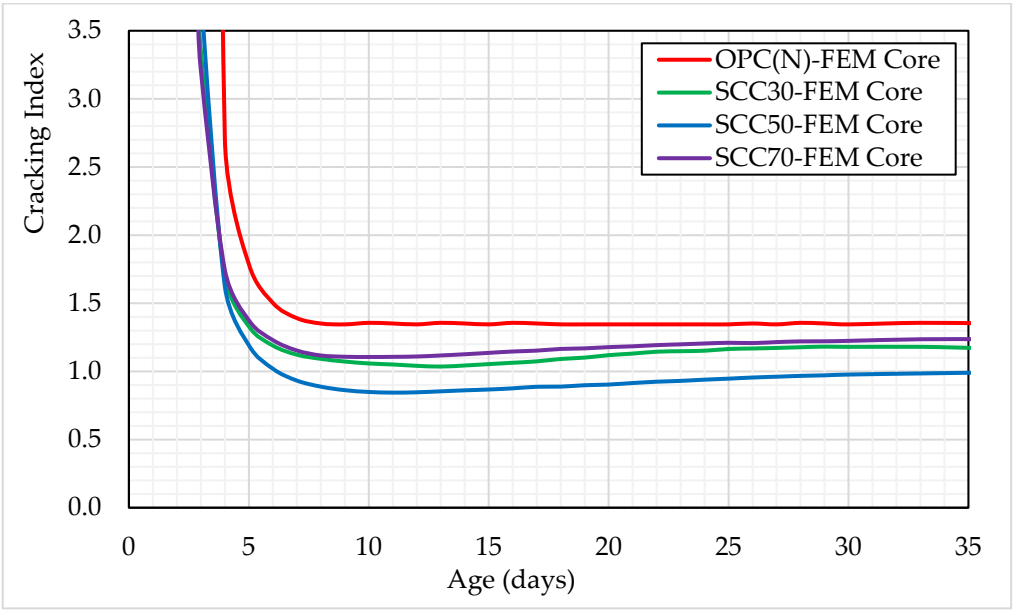


Figure 25. Cracking index of the concrete wall structure at an early age.

3.6.3. Cracking Resistance of Massive SCC Concrete Subjected to Drying Age

When concrete is subjected to drying, drying shrinkage stresses are superimposed on thermal stresses and autogenous shrinkage stress. In this case, the critical cracking tendency region shifts from the core to the surface of the structure, as shown in Figure 26. Drying shrinkage becomes the predominating factor, and critical cracking regions occur at the surface of the member.

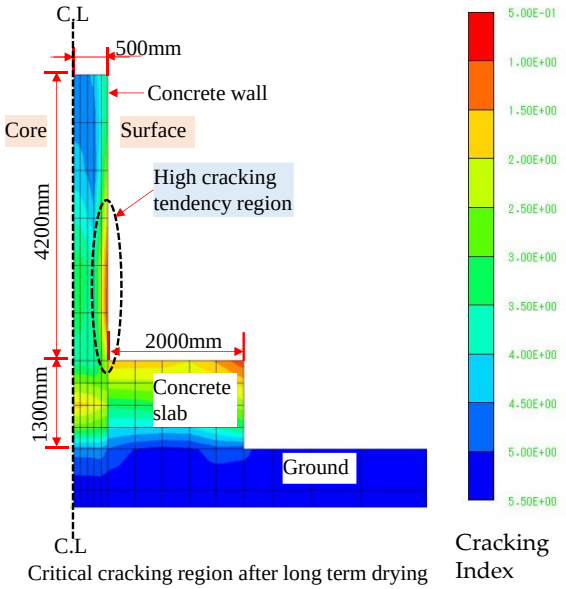


Figure 26. Critical cracking region of the concrete wall at extended drying age.

Stress analysis results of the massive SCC concrete structure exposed to drying are shown in Figure 27a and Figure 27b for the core and surface, respectively.

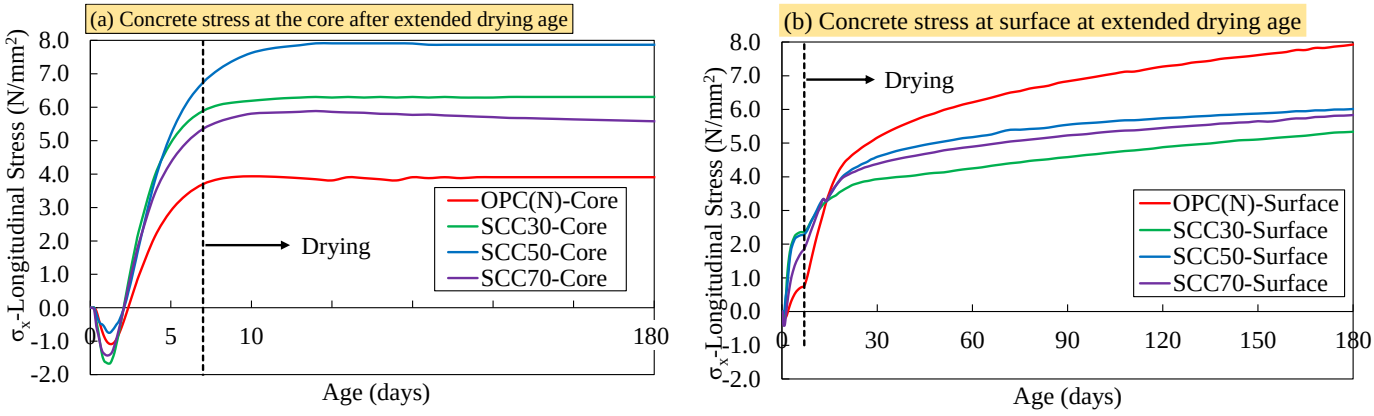


Figure 27. Stresses at the core and surface of the concrete subjected to drying.

Results show that SCC50 experiences the highest stresses. This is because of the high heat of hydration and autogenous shrinkage associated with it. At the core, OPC has low stresses. This is due to a low temperature rise and low autogenous shrinkage. When the structure is subjected to drying for up to 6 months, the trend at which stress is developed in the surface changes. Stress increases gradually as time increases. In the case of self-compacting concrete, SCC50 has the highest stresses. SCC70, however, becomes the second most critical while SCC30 develops low stresses. SCC30 has the lowest stress, and this is largely due to its low autogenous shrinkage, as explained earlier.

As drying continues, a critical region with low cracking resistance is at the surface of the wall. Analysis results of the concrete cracking index at the surface of the wall after prolonged drying are shown in Figure 28. When subjected to drying, the surface of the concrete becomes critical. Considering the cracking index at the surface of the structure, the trend is different from that at the core.

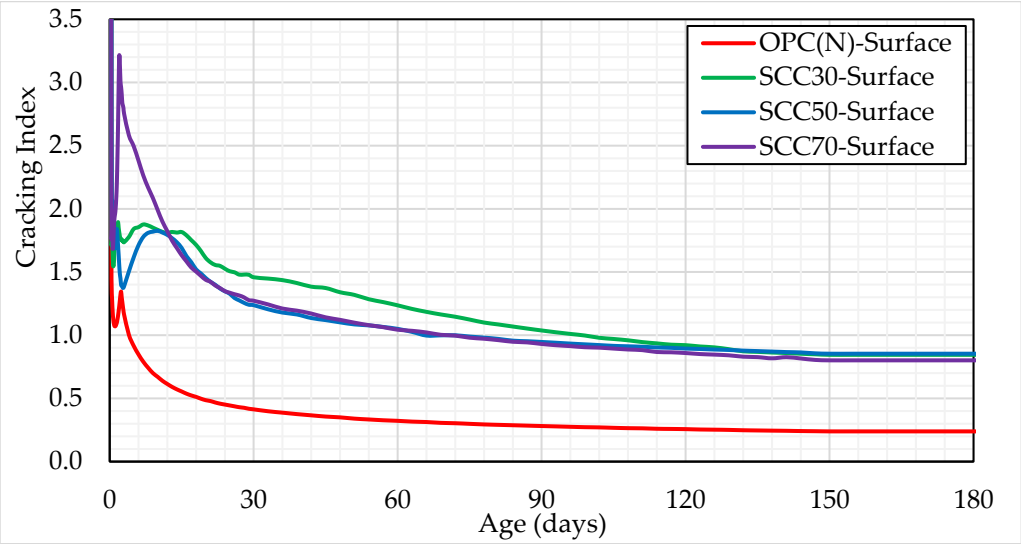


Figure 28. Cracking index at the surface of the concrete wall subjected to drying.

At 6 months of drying age, SCC50 has a high cracking index, indicating that as drying continues, it becomes better in cracking resistance than SCC30 and SCC70. This is because SCC50 has a higher 28-day compressive than SCC30. This influences the calculation of splitting tensile strength, which is used to calculate the cracking index. This shows that the cracking resistance of each mix proportion may also depend on the exposure condition of the structure and its strength at the control age (28 days). Research by Amir Hossein and Mahmoud Nili also showed that self-compacting concrete is better than OPC concrete in crack resistance when subjected to extended drying conditions [40].

4. Conclusions

1. A new reduction coefficient for effective modulus of elasticity is proposed to precisely evaluate the influence of drying shrinkage on restraint stress using 3D FEM;
2. From FEM analysis of wall-type structures, it is proven that the optimum blast furnace slag replacement for massive self-compacting concrete for better-cracking resistance depends on the expected exposure condition of the structure;
3. Partial replacement of blast furnace slag contributes to low temperature and improved cracking resistance at an early age while drying shrinkage influences cracking resistance;
4. Self-compacting concrete performs better than OPC concrete in concrete cracking resistance when subjected to drying for up to 6 months.

Author Contributions: All authors contributed to the planning, design, experiments, and writing this paper as follows: Conceptualization and methodology; B.K. and S.M., Formal analysis; B.K. and S.M., writing paper—original draft, review, and editing; B.K. and S.M., Project administration, supervision, and validation; S.M. All authors have read and agreed to the published version of the manuscript.

Funding: This research received no external funding.

Data Availability Statement: All data generated and analyzed during this study are included in this article.

Acknowledgments: The authors of this paper wish to acknowledge the immeasurable support given by the Japan International Cooperation Center (JICE) through The Project for Human Resource Development Scholarship Program—JDS.

Conflicts of Interest: The authors declare no conflicts of interest.

References

1. Ouchi, M.; Nakamura, S.-A.; Osterberg, T.; Lwin, M. Applications of Self-Compacting Concrete in Japan, Europe and The United States. In Proceedings of the International Symposium on High Performance Computing, Tokyo, Japan, 20–22 October 2003.
2. Liu, D.; Zhang, Z.; Zhang, X.; Chen, Z. 3D printing Concrete Structures: State of the art, Challenges, and Opportunities. *Constr. Build. Mater.* **2023**, *405*, 133364. [CrossRef]
3. Jang, I.; Maruyama, I. Numerical Prediction of Crack Width in Massive Concrete Member Due to Heat of Hydration. In Proceedings of the JCI-RILEM International Workshop on "Control of Cracking of Mass Concrete and Related Issues Concerning Early Age Cracking of Concrete Structures" (CONCRACK5), Tokyo, Japan, 24–26 April 2017.
4. Rozière, E.; Granger, S.; Turcry, P.; Loukili, A. Influence of paste volume on shrinkage cracking and fracture properties of self-compacting concrete. *Cem. Concr. Compos.* **2007**, *29*, 626–636. [CrossRef]
5. Al Rifai, M.M.; Sikora, K.S.; Hadi, M.N. Effect of micro steel fibers volume fraction on behavior of high-strength self-compacting concrete. *Constr. Build. Mater.* **2024**, *450*, 138709. [CrossRef]
6. Yang, Q.; Zeng, L.; Wang, H.; Xiang, R.; Guan, L.; Cheng, J. Influence of Extra-Short Extra-Fine Steel Fibers on Mechanical Properties of Self-Compacting Concrete with Single-Doped Fly Ash. *Buildings* **2024**, *14*, 1396. [CrossRef]
7. Shi, C.; Wu, Z.; Lv, K.; Wu, L. A review on mixture design methods for self-compacting concrete. *Constr. Build. Mater.* **2015**, *84*, 387–398. [CrossRef]
8. Leonhardt, F. Cracks and Crack Control in Concrete Structures. *PCI J.* **1988**, *33*, 124–145. [CrossRef]
9. Hanein, T.; Galvez-Martos, J.L.; Bescher, E. The Role of Belitic Calcium Sulfoaluminate Cement in Achieving Net-Zero. In Proceedings of the 16th International Congress on the Chemistry of Cement 2023—ICCC2023, Thailand, Bangkok, 18–22 September 2023.
10. Kipkemboi, B.; Miyazawa, S. Properties and Thermal Stress Analysis of Blended Cement Self-Compacting Concrete. *Open J. Civ. Eng.* **2018**, *8*, 102–120. [CrossRef]
11. Khatib, J.M. Performance of self-compacting concrete containing fly ash. *Constr. Build. Mater.* **2008**, *22*, 1963–1971. [CrossRef]
12. Klemczak, B.; Gołaszewski, J.; Smolana, A.; Gołaszewska, M.; Cygan, G. Shrinkage behaviour of self-compacting concrete with a high volume of fly ash and slag experimental tests and analytical assessment. *Constr. Build. Mater.* **2023**, *400*, 132608. [CrossRef]
13. Cha, S.-L.; Jin, S.-S. Prediction of thermal stresses in mass concrete structures with experimental and analytical results. *Constr. Build. Mater.* **2020**, *258*, 120367. [CrossRef]
14. Aghiad, A.; Miyazawa, S.; Nito, N.; Kuga, R.; Sakai, E. Cracking Resistance of Steam-Cured Precast Concrete Using High Alite Cement with Modified Fly Ash. *Infrastructures* **2023**, *8*, 154. [CrossRef]
15. Tang, S.; Huang, D.; He, Z. A review of autogenous shrinkage models of concrete. *Build. Eng.* **2021**, *44*, 103412. [CrossRef]
16. Turcry, P.; Loukili, A.; Haidar, K.; Pijaudier-Cabot, G.; Belarbi, A. Cracking Tendency of Self-Compacting Concrete Subjected to Restrained Shrinkage: Experimental Study and Modelling. *J. Mater. Civ. Eng.* **2006**, *18*, 46–54. [CrossRef]
17. Nijs, K.; Ishikawa, M. Finite Element Implementation of a Drying Shrinkage Model Based on Pore Evaporation Mechanics. In Proceedings of the High Tech Concrete: Where Technology and Engineering Meet—Proceedings of the 2017 fib Symposium, Maastricht, The Netherlands; 2017.
18. Japan Concrete Institute. *Guideline for Control of Cracking of Mass Concrete*; Japan Concrete Institute: Tokyo, Japan, 2008.
19. Guojie, W.; Jiding, L.; Jianlan, Z.; Wei, F. Study on the stress relaxation properties of self-compacting concrete under restrained autogenous shrinkage. *IOP Conf. Ser. Mater. Sci. Eng.* **2018**, *431*, 102010. [CrossRef]
20. Ryoichi, A.; Mizobuchi, T.; Izumi, H. Evaluation for Apperent Instantaneous Stiffness Decrease Considering Effect of Creep of Early Age Concrete. *Cem. Sci. Concr. Technol.* **2019**, *73*, 200–207.
21. JSCE. *Standard Specifications for Concrete Structures*; Japan Society of Civil Engineers: Tokyo, Japan, 2012.
22. *ASTM C33*; Standard Specification for Concrete Aggregates. In Annual Book of ASTM Standards. ASTM International: West Conshohocken, PA, USA, 2003.
23. Japan Society of Civil Engineers. *Recommendation for Mix Design and Construction of Self Compacting Concrete*; Japan Society of Civil Engineers: Tokyo, Japan, 2012.
24. *ASTM C39*; Standard Test Method for Compressive Strength of Cylindrical Concrete Specimen. ASTM International: West Conshohocken, PA, USA, 2002.
25. Yasuyuki, K.; Hirotaka, K.; Hiroshi, W. A Study on estimation of adiabatic temperature rise charcteristics of high strength concrete by simple adiabatic test. In Proceedings of the 57th Annual Conference of Japan Society of Civil Engineering, Sapporo, Japan, 25–27 September 2002.
26. Japan Concrete Institute. *Guideline for Control of Cracking of Mass Concrete 2016*; Japan Concrete Institute: Tokyo, Japan, 2017.
27. Japan Concrete Institute. *Autogenous Shrinkage of Concrete*, 1st ed.; Tazawa, E., Ed.; CRC Press: London, UK, 1999.
28. Kipkemboi, B.; Zhao, T.; Miyazawa, S.; Sakai, E.; Nito, N.; Hirao, H. Effects of C3S content of clinker on properties of fly ash cement concrete. *Constr. Build. Mater.* **2020**, *240*, 117840. [CrossRef]

29. *ASTM C157/157M*; Standard Test Method for Length Change of Hardened Hydraulic Cement Mortar and Concrete. ASTM International: West Conshohocken, PA, USA, 2008.
30. Lim, C.-K.; Kim, J.-K.; Seo, T.-S. Prediction of concrete adiabatic temperature rise characteristic by semi-adiabatic temperature rise test and FEM analysis. *Constr. Build. Mater.* **2016**, *125*, 679–689. [CrossRef]
31. Wang, J.; Zhang, J.; Zhang, J. Cement Hydration Rate of Ordinarily and Internally Cured Concretes, Wuhan University of Technology—Material Science Edition. *J. Adv. Concr. Technol.* **2018**, *16*, 306–316. [CrossRef]
32. Yang, Y.; Sato, R.; Kawai, K. Evaluation of autogenous shrinkage and drying shrinkage based on bound water content of cementitious materials, in JSCE Preceedings. *Doboku Gakkai Ronbunshu* **2001**, *2001*, 109–120. [CrossRef]
33. American Concrete Institute. ACI Concrete Terminology. In *American Concrete Institute—Advancing Concrete Knowledge*; American Concrete Institute: Farmington Hills, MI, USA, 2013.
34. Abdalhmid, J.M.; Ashour, A.; Sheehan, T. Long-term drying shrinkage of self-compacting concrete: Experimental and analytical investigations. *Constr. Build. Mater.* **2019**, *202*, 825–837. [CrossRef]
35. Xie, S.; Cheng, Z.; Wan, L. Hydration and Microstructure of Astm Type I Cement Paste. *Sci. Eng. Com. Mater.* **2019**, *26*, 215–220. [CrossRef]
36. Qu, Z.; Si, R.; Jia, P.; Zhang, Y. Creep and relaxation responses of fly ash concrete: Linear and nonlinear cases. *Case Stud. Constr. Mater.* **2022**, *17*, e01562. [CrossRef]
37. Yamada, H.; Katahira, H.; Watanabe, H. Estimation for Drying Shrinkage of Concrete by Composite Model using Coarse Aggregate Properties. *J. Jpn. Soc. Mater. Sci.* **2018**, *67*, 396–400. [CrossRef]
38. Imamoto, K.-I. Simplified Prediction of Drying Shrinkage Stress in Reinforced Concrete Building Wall. *J. Adv. Concr. Technol.* **2008**, *6*, 111–120. [CrossRef]
39. Ippei, M. Impact of drying on Concrete and Concrete Structures. *Rilem Tech. Lett.* **2022**, *7*, 1–11.
40. Ghorbankhani, A.H.; Nili, M. Experimental and numerical assessment of thermal properties of self-compacting mass concrete at early ages. *Eur. J. Environ. Civ. Eng.* **2021**, *26*, 8194–8211. [CrossRef]

Disclaimer/Publisher's Note: The statements, opinions and data contained in all publications are solely those of the individual author(s) and contributor(s) and not of MDPI and/or the editor(s). MDPI and/or the editor(s) disclaim responsibility for any injury to people or property resulting from any ideas, methods, instructions or products referred to in the content.